Design of the Hybrid Wing Body with Nacelle: N3-X Propulsion-Airframe Configuration

[1]Hyoungjin Kim
SAIC, Cleveland, Ohio, 44135

David Harding[2]
University of Texas at Austin, Austin, Texas, 78705

David T. Gronstal[3]
The University of Alabama, Tuscaloosa, Alabama, 35401

May-Fun Liou[4] and Meng-Sing Liou[5]
NASA Glenn Research Center, Cleveland, Ohio, 44135

Abstract

The Hybrid Wing Body (HWB) aircraft is of great interest for future transport concepts due to its promises of reduced aircraft noise, nitrous-oxide emissions, and fuel consumption. A design parameterization method for HWB configurations with mail slot nacelle has been developed for a fast exploration of design space in conceptual and preliminary design phases of a HWB configuration. A HWB planform model by Laughlin[11] was implemented, and the Class Shape Transformation (CST) airfoil generation method by Kulfan[10] was utilized to construct the needed geometry for computational high fidelity aerodynamic simulations. Geometric constraints for the parameterization such as internal cabin and cargo hold layouts were imposed on the geometry generation. A CFD simulation was performed for a HWB configuration generated by the current geometric modeler, clearly showing a significant effect of the installed nacelle on the flowfield.

Nomenclature

ζ_{up}	=	Nondimensional CST z coordinates for airfoil upper surface
ζ_{low}	=	Nondimensional CST z coordinates for airfoil lower surface
η	=	Nondimensional y coordinates
η_{local}	=	Nondimensional local y coordinate
Λ_1	=	Sweep angle of the leading edge of the planform
Λ_2	=	Sweep angle of the outboard wing of the planform
λ_1	=	Coefficient representing the distance between the cabin body and the root chord of the outboard wing
λ_2	=	Coefficient representing the reach of the curved section of the leading edge of the outboard wing
λ_3	=	Coefficient representing the reach of the curved section of the trailing edge of the outboard wing
ξ_{un}	=	Nondimensional trailing edge thickness for the upper surface of the nth control airfoil on the aircraft
ξ_{ln}	=	Nondimensional trailing edge thickness for the lower surface of the nth control airfoil on the aircraft
ψ	=	Nondimensional CST x coordinates
A_u	=	CST optimization variable vector for the upper surface of the airfoil
A_l	=	CST optimization variable vector for the lower surface of the airfoil

[1] Aerospace Engineer. Senior Member AIAA
[2] Engineering Intern (2013), Propulsion Division.
[3] Engineering Intern (2014), Propulsion Division.
[4] Aerospace Engineer, Propulsion Division. Senior Member AIAA
[5] Senior Technologist, Propulsion Division. Fellow AIAA

b_{ow} = Span of the outboard wing
b = Total span
c_{local} = Local chord length
$c_{r,cb}$ = Root chord of the cabin body
$c_{r,ow}$ = Root chord of the outboard wing
$c_{t,cb}$ = Tip chord of the cabin body
$c_{t,ow}$ = Tip chord of the outboard wing
h = Offset vector of the control airfoils for the aircraft
$h_{nacelle}$ = Height of the nacelle as referenced from the surface of the aircraft
l_{cb} = Length of the cabin body
N = Bernstein polynomial order for CST airfoil generation of the aircraft
N_1 = Class function exponent for CST airfoil generation of the aircraft
N_2 = Class function exponent for CST airfoil generation of the aircraft
w_{cb} = Width of the cabin body
x_{LE} = Leading edge position vector
X = Dimensionalized CST x coordinates
Y = Dimensionalized CST y coordinates
Z_{up} = Dimensionalized CST z coordinates for airfoil upper surface
Z_{low} = Dimensionalized CST z coordinates for airfoil lower surface

I. Introduction

Hybrid Wing Body (HWB) aircraft is characterized by a flattened and airfoil-shaped body, which produces a substantial portion of the total lift. The body form is composed of distinct and separate wing structures, though the wings are smoothly blended into the body. This concept has been studied widely and results suggest remarkable performance improvements over the conventional tube and wing transport[1,2]. HWB incorporates design features from both a futuristic fuselage and flying wing design, which houses most of the crew, payload and equipment inside the main centerbody structure. The purported advantages of the HWB approach are efficient high-lift wings and a wide-shaped body, which together reduce the wing loading and boost the spanwise lift distribution. This enables the entire craft to contribute to lift generation with the result of potentially increased fuel efficiency and range; the smoothly blended wing-body reduces interference drag. In addition, the wide airfoil-shaped body has demonstrated shielding downward propagating noise from the engines mounted on the upper surface of the vehicle[3]. Lyu et al.[4] pointed out the challenges in designing HWB and reviewed major studies done in design optimization of the HWB configuration. Those efforts are very important in designing the unconventional HWB due to the fact that little historical data can be drawn, unlike the conventional tube-and-wing transport aircraft. However, the embedded engines in HWB vehicle, instead of pylon-mounted engine, would be partly submerged in boundary layer from center body upstream of the inlet with boundary-layer-ingestion (BLI) offset inlet employed. The BLI offset inlet provides better propulsion efficiency by reducing form drag, wetted area, structural weight and noise. However, the higher flow distortion and lower pressure recovery at the Aerodynamic Interface Plane (AIP) found in the BLI offset inlet are disadvantages[5]. Consequently the low momentum flow at the low recovery region within the highly distorted flows may separate inside the diffuser and results in insufficient air supply to fan face[6]. Moreover, the installation of the nacelle is shown to significantly degrade the potential of the highly desirable aerodynamic efficiency of HWB in clean wing, see Ref. [7]. Hence, the main premise of the present work is to develop a design approach that includes both the airframe and propulsion systems at the outset of aerodynamic design of the aircraft. A similar propulsion-airframe integration (PAI) design approach was conducted on an over-wing nacelle airliner configuration[8]. This paper will illustrate an efficient geometric parameterization of a complex propulsion-airframe integration of the HWB, using the N3-X[9,10] hybrid wing-body with a mail-slot inlet/nozzle nacelle as a test case.

To determine the optimal aerodynamic performance of the aircraft, a geometric model represented by a set of parameters (design variables) must be created in which these design variables can be quickly and easily altered. The Class Shape Transformation (CST) [11], a non-dimensional airfoil generation method, is utilized to construct the needed geometry for preliminary aerodynamic testing. The remainder of this paper is organized as follows. Section II illustrates the geometry definition of HWB planform and its associated parameters by using CST. Section III presents our geometric representation of HWB clean wing body and nacelle, including the validation with the N3-X clean wing body. Section IV gives the demonstration of aerodynamic analysis from the computational fluid

dynamics (CFD) simulations. In this study, we employ GO-flow[9], a high-fidelity Euler / Navier-Stokes flow solver. Finally, concluding remarks are given in Section V.

II. HWB Planform Overview

The planform is the two-dimensional shadow of the aircraft as viewed from a position directly above the craft. It is an ideal starting point for the design because it serves as the two-dimensional basis by which the CST method can be employed to generate the three-dimensional aircraft body. The following HWB planform design was partially derived from the work of Laughlin's[11] with the HWB planform.

A. Definition of Planform Shape

Shown in Fig. 1 is the HWB planform with all control points labeled. The inboard sections of the aircraft planform are defined via splines passing through the inboard control points and the outboard sections are defined linearly. Here, a cubic spline for [y1, y3], through the first three (control) points and a linear spline through the last two are created. Details for the determination of the leading edge and trailing edge splines are given in Appendix A.

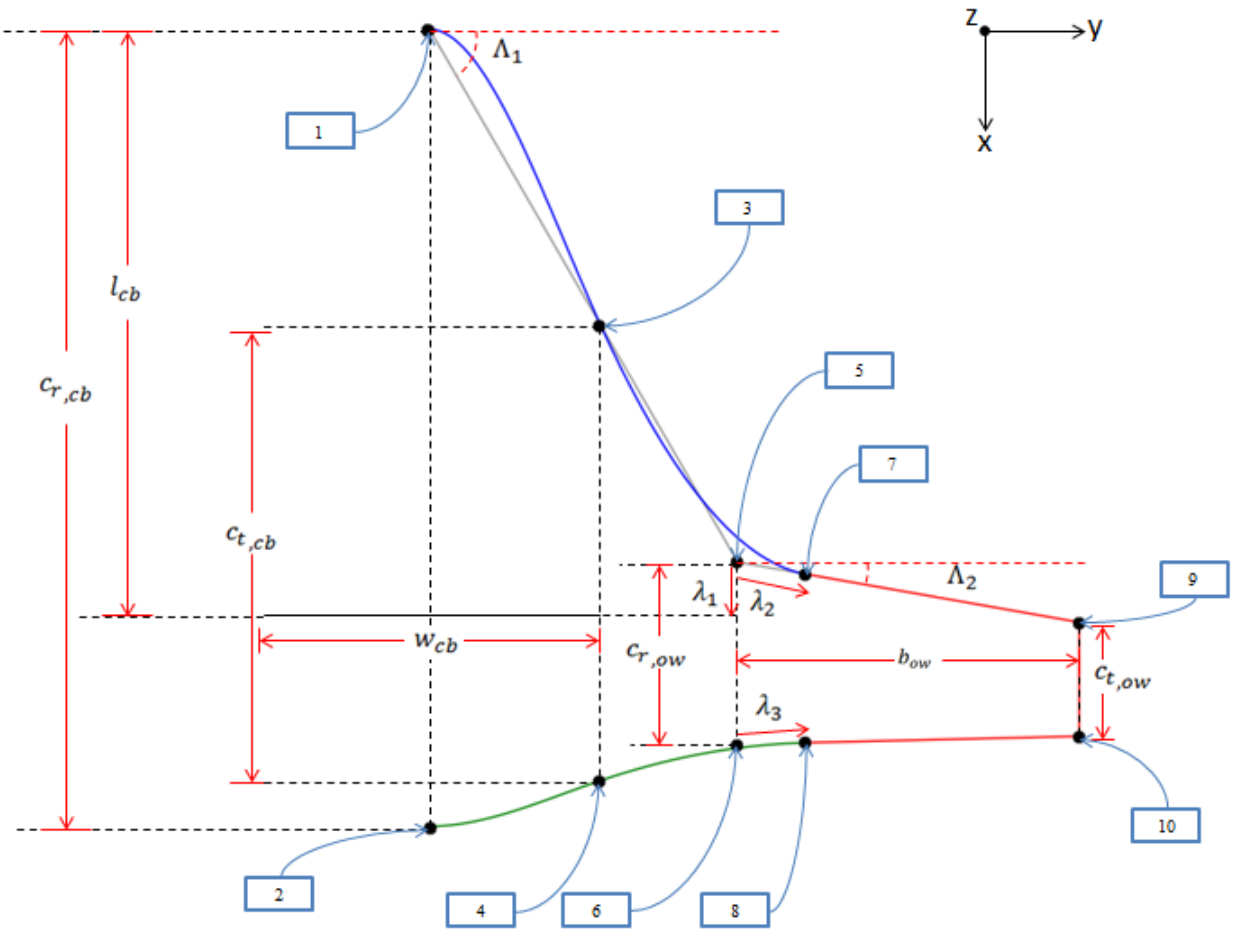

Figure 1: Planform definition of Hybrid Wing Body configuration

B. Planform Control Points

The HWB aircraft planform is composed of ten control points whose locations are derived from the twelve planform design variables: $c_{r,cb}$, $c_{t,cb}$, $c_{r,ow}$, $c_{t,ow}$, w_{cb}, l_{cb}, b_{ow}, Λ_1, Λ_2, λ_1, λ_2, and λ_3. These ten control points, (x_1,y_1) to (x_{10},y_{10}), are found through solving the following two systems of linear equations: Eqs. (1)-(10) for the x coordinates and Eqs. (11)-(20) for the y coordinates.

$$x_1 = 0 \tag{1}$$

$$x_2 = x_1 + c_{r,cb} \tag{2}$$

$$x_3 = x_1 + \frac{1}{2} w_{cb} \tan(\Lambda_1) \tag{3}$$

$$x_4 = x_3 + c_{t,cb} \tag{4}$$

$$x_5 = l_{cb} - \lambda_1 c_{r,ow} \tag{5}$$

$$x_6 = x_5 + c_{r,ow} \tag{6}$$

$$x_7 = x_5 + \lambda_2 b_{ow} \tan(\Lambda_2) \tag{7}$$

$$x_8 = \lambda_3 (x_{10} - x_6) + x_6 \tag{8}$$

$$x_9 = x_5 + b_{ow} \tan(\Lambda_2) \tag{9}$$

$$x_{10} = x_9 + c_{t,ow} \tag{10}$$

$$y_1 = 0 \tag{11}$$

$$y_2 = y_1 \tag{12}$$

$$y_3 = y_1 + \frac{1}{2} w_{cb} \tag{13}$$

$$y_4 = y_3 \tag{14}$$

$$y_5 = \frac{l_{cb} - \lambda_1 c_{r,ow}}{\tan(\Lambda_1)} \tag{15}$$

$$y_6 = y_5 \tag{16}$$

$$y_7 = y_5 + \lambda_2 b_{ow} \tag{17}$$

$$y_8 = \lambda_3 (y_{10} - y_6) + y_6 \tag{18}$$

$$y_9 = y_5 + b_{ow} \tag{19}$$

$$y_{10} = y_9 \tag{20}$$

III. The Clean Wing HWB Aircraft and Nacelle

III-1 : The Clean Wing HWB Aircraft

The first step in the generation of the three-dimensional HWB aircraft is the creation of the clean airframe. This is the body of the aircraft sans any additional external features, such as nacelles. To generate the clean wing body, four control sectional airfoils are placed along the spanwise direction at y1, y3, y7 and y9, respectively.

The airfoil shape at each design section is generated by the CST method. Although the CST method can be used either in one-dimensional formulation for airfoils or two-dimensional formulation for wing shapes, in this study the design section airfoils are defined by the two-dimensional CST formulation, and the sectional shapes between the design sections are generated by interpolation of CST parameters at the two design sections. This is because the HWB configuration has abrupt change in sectional shapes in the spanwise direction that is hard to capture with only four design sections.

A. Control Airfoils

The control airfoils are the elements within the HWB aircraft design that determine the three-dimensional shape of the aircraft. They are created through the employment of the CST method and dimensionalized based on planform locational parameters. When defining the nondimensional airfoil shape, a nondimensional local x coordinate, ψ, is created; ψ is identical for each control airfoil and is defined as a nondimensional chord line that is equal to zero at the leading edge of the airfoil and one at the trailing edge. Once ψ is defined, the CST method can be employed to determine the nondimensional z coordinates, ζ_{up} and ζ_{low}. ζ_{up} and ζ_{low} are defined for the nth control airfoil by Eqs. (21) and (22), representing the CST method.

$$\zeta_{up} = \psi^{N_1}(1-\psi)^{N_2}\sum_{i=0}^{N}\left(A_{u_i}\left(\frac{N!}{i!\,(N-i)!}\right)\psi^{i}(1-\psi)^{(N-i)}\right) + \psi\xi_u \tag{21}$$

$$\zeta_{low} = \psi^{N_1}(1-\psi)^{N_2}\sum_{i=0}^{N}\left(A_{l_i}\left(\frac{N!}{i!\,(N-i)!}\right)\psi^{i}(1-\psi)^{(N-i)}\right) + \psi\xi_l \tag{22}$$

In Eqs. (21) and (22), A_{u_i} and A_{l_i} refer to the i[th] value of the design parameter vector for the upper and lower surfaces of the section airfoil, and ξ_u and ξ_l refer to the nondimensionalized twist. Here $\xi_u = \xi_l$ so that sectional airfoils have zero trailing edge thickness.

To dimensionalize each sectional airfoil shape, the local chord length is used for x and z coordinates and the total span is used for the y coordinates. The η term is not used in airfoil generation; it is used solely to determine the spanwise location of each airfoil. Furthermore, the x and z coordinates each have an offset term added to them. The x coordinates have an offset term corresponding to the leading edge position of each respective CAF; this offset is a function of the planform. The z coordinates have an offset that is used to counteract the fact that the CST method defines the leading edge z coordinate at z = 0. This z offset can be utilized to create such designs as a dihedral or anhedral wing aircraft. The dimensionalizing procedure is shown in Eqs. (23)-(26). η is defined as 0 at the symmetric section and 1 at the wing tip.

$$X = \psi c_{local} + x_{LE} \tag{23}$$

$$Y = 0.5\eta b \tag{24}$$

$$Z_{up} = \zeta_{up} c_{local} + h \tag{25}$$

$$Z_{low} = \zeta_{low} c_{local} + h \tag{26}$$

In this study, the number of design parameters is set as seven, thus N = 6 in Eqns. (21) and (22). As the initial sectional airfoil shape in this study, the sectional shapes of the N3-X configuration [9] is extracted and fitted by the CST method by gradient-based optimization. Figure 2 shows the results for the curve fitting for airfoils at sections η =0, 0.3, 0.7, and 1.0 of the N3-X airframe.

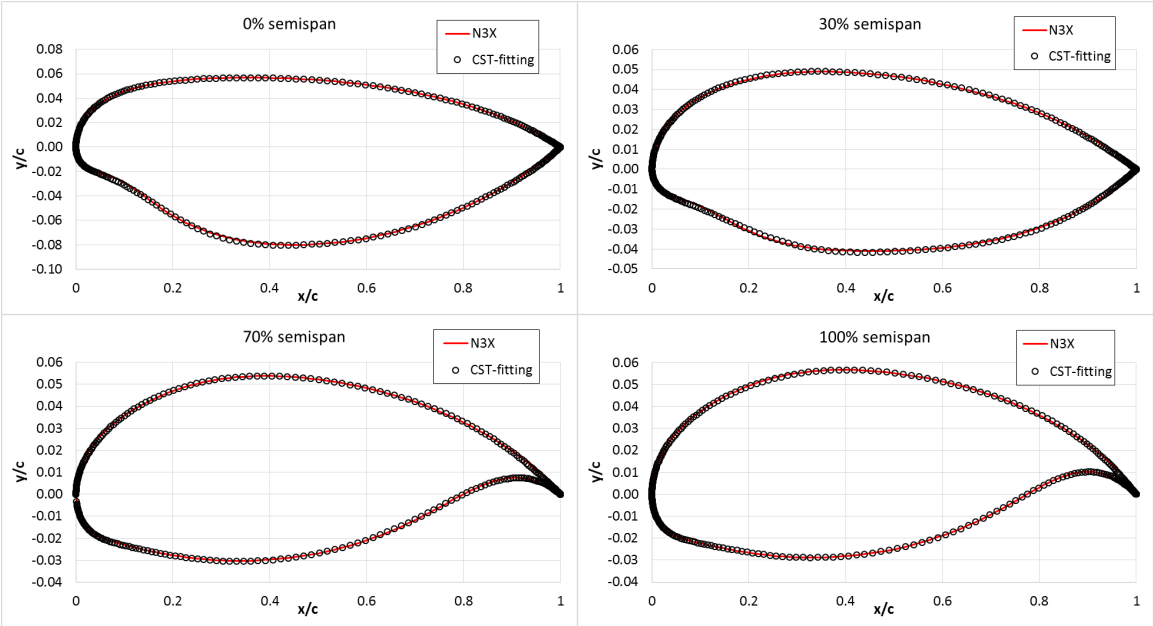

Figure 2: CST Control Airfoils for the Hybrid Wing Body Aircraft

B. Interpolation of sectional airfoil shapes

At any given spanwise location, the sectional airfoil must have its own set of unique CST parameters, twist, and z-offset values. A linear interpolation of the design parameters between two design sections was adopted for efficient determination of the parameters. However, it is important to note that the interpolated sectional airfoils are not simply linear interpolations of the design sectional airfoils. Since each airfoil is dimensionalized based on planform locational variables such as local chord length and spanwise position, the interpolated sectional airfoils create a smooth, planform-dependent, blended transition between any two design sectional airfoils.

The CST parameters are determined via interpolation based on a local non-dimensional y coordinate, η_{local}. When doing this interpolation in the middle of two design sections, the design section closer to the root chord is defined as $\eta_{local} = 0$ and the design section closer to the tip is defined as $\eta_{local} = 1$. This definition provides for an extremely simple linear interpolation of design variables, as shown in Eqs. (27)-(31).

$$\xi_u = \xi_{0,u} + (\xi_{1,u} - \xi_{0,u})\eta_{local} \tag{27}$$

$$\xi_l = \xi_{0,l} + (\xi_{1,l} - \xi_{0,l})\eta_{local} \tag{28}$$

$$h = h_0 + (h_1 - h_0)\eta_{local} \tag{29}$$

$$A_u = A_{0,u} + (A_{1,u} - A_{0,u})\eta_{local} \tag{30}$$

$$A_l = A_{0,l} + (A_{1,l} - A_{0,l})\eta_{local} \tag{31}$$

Once the design parameters are obtained they are passed to Eqs. (21) and (22) to find the nondimensional z coordinates for each section airfoil. Following this, Eqs. (23)-(26) are utilized to dimensionalize each section airfoil. A front view and an isoperimetric view of the clean wing HWB aircraft is shown in Fig. 3 and Fig. 4, respectively.

Figure 3: Front View of the Clean Wing Hybrid Wingbody Aircraft

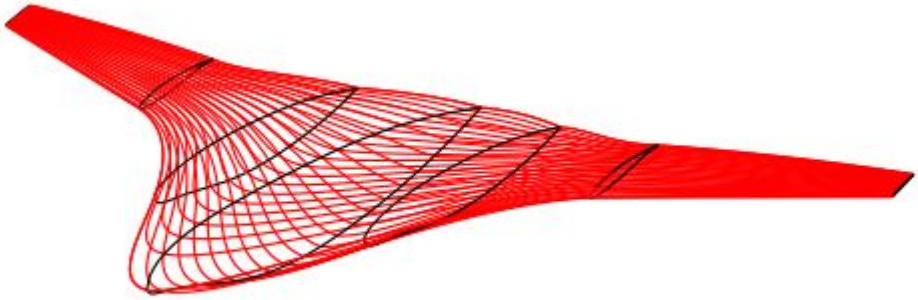

Figure 4: Isoperimetric View of the Clean Wing Hybrid Wing-body Aircraft

III-2 Mail Slot Nacelle

The final step in generating the geometry of the HWB aircraft is to create the nacelle. The nacelle for the N3-X HWB aircraft is dubbed the "mail-slot" nacelle. It is located on the upper surface of the aircraft (thus aiding in noise reduction because the actual body of the aircraft creates a shield for the noise) and houses the propulsion system. It was given the name "mail-slot" nacelle due to the fact that actual nacelle structure bears resemblance to a mail-slot.

A. Nacelle Geometry

The nacelle geometry was first generated with a straight leading edge and trailing edge. Translational movements can be made in the chordwise direction for any given nacelle planform on the airframe. Also, rotational movements for each sectional airfoil of the nacelle is required so the nacelle is aligned with the local slope of the airframe upper surface at the installation location. In this study, it was assumed that the mail slot nacelle has constant chord length along the span of the nacelle, and the nacelle trailing edge follows the trailing edge of the airframe. This assumption can be easily changed when needed.

This procedure is the same as our previous work [9] for mail slot nacelle geometry generation with all the flow passages inside the nacelle. The difference is that the current nacelle has a simplified geometry with a single flow passage for the mail slot instead of having many number of internal flow passages or center body for propulsive fan installation. This simplified nacelle geometry is for fast turnaround time for geometry modeling and high fidelity flow simulations at conceptual and preliminary design phases of the HWB configuration with mail-slot nacelle, while keeping aerodynamic effects of the existence of mail slot on the airframe. The single passage is not a flow-through passage, but terminated by a boundary plane for numerical boundary conditions of specifying back pressure for a subsonic exit flow condition. The exit of the nacelle has another single plane for nozzle exit boundary condition as shown in Fig. 5.

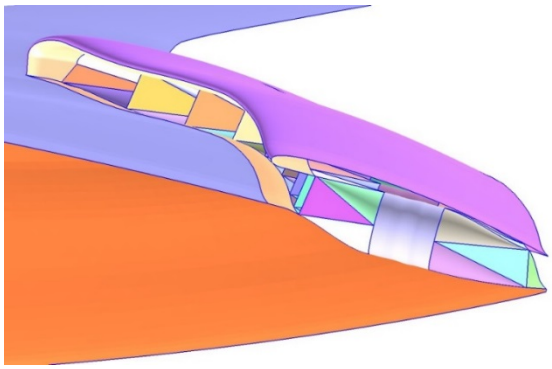

(a) Full geometry of mail-slot nacelle with eight flow passages in the half model

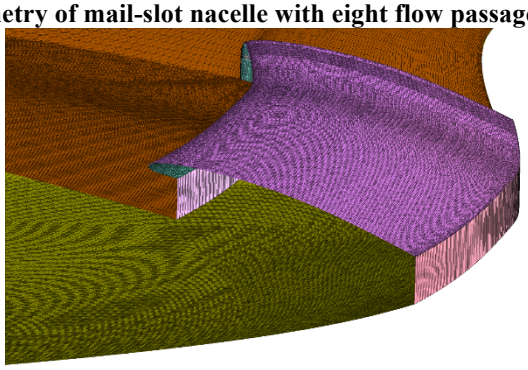

(b) Simplified mail-slot nacelle Structure

Figure 5: Mail-slot nacelle geometry

B. Formulating the Mail-slot Shape

The three dimensional shape of the nacelle is mail-slot shaped, as noted above; the nacelle planform sits at a height $h_{nacelle}$ above the surface of the HWB aircraft. Therefore, the height of the nacelle is a function of the upper surface of the aircraft. Due to this, legs and rounded edges connecting the legs to the planform must be defined. The rounded edges are created as quarter ellipses in the y-z plane. Thus the nacelle legs have a height that is equivalent to the difference between the planform height at the nacelle edges and the height of the ellipse. Fig. 5 shows the mail-slot shape of the nacelle.

Figure 6 shows a front view of the mail slot nacelle installed on the airframe. The figure clearly shows the horizontal region, quarter ellipse region and vertical leg region of the nacelle.

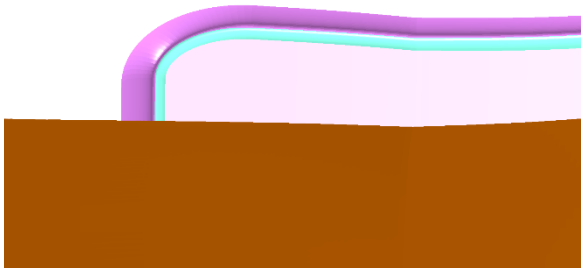

Figure 6: Front view of mail slot nacelle: horizontal, quarter elliptic, and vertical leg regions of the nacelle cowl are clearly seen.

C. Nacelle Airfoil Sections

To promote aerodynamic efficiency, the cross section of the mail slot nacelle is also airfoil shaped. Therefore, the cross section of the nacelle can be created exactly as the control airfoils were created. The primary difference is that the nacelle airfoils are generated by three-dimensional formulation [10] of CST because of smooth variation of sectional shapes of the mail slot nacelle.

IV. Geometric Constraints for HWB Airframe

The airframe outer mold line (OML) defined by the present HWB planform and sectional shape parameterization has to be defined so that the airframe wraps around the internal cabin and cargo hold without any intersection with the internal volumetric structures. In order to specify the geometric constraints on the airframe configuration, the HWB cabin layout suggested by Nickol [12] for 301 passengers shown in Fig. 7 was adopted here. Based on the layout of the cabin design and height of the cabin suggested by Nickol, we generated a volumetric model of cabin and cargo hold as shown in Fig. 8. Design parameters such as the airframe planform, sectional airfoil thicknesses, and even the dimensions of the cargo hold were adjusted so that there is no intersection between the OML and the internal frames. The volume of the cargo hold was kept larger than the required volume of 5656 ft^3, which is the cargo hold volume of Boeing 777-200LR. The root chord length of the HWB configuration is 118 ft, and the leading edge sweep angle of centerbody is set as 51 degrees following the cabin sweep angle in Fig. 7(a). As mentioned earlier, the sectional shapes are the same as the N3-X configuration [9] as shown in Fig. 2, and the maximum thicknesses of the design sections are used as additional design parameter.

The HWB configuration in Fig. 8 is not any result of shape design optimization, but just a demonstration of the geometric parameterization method of the present study.

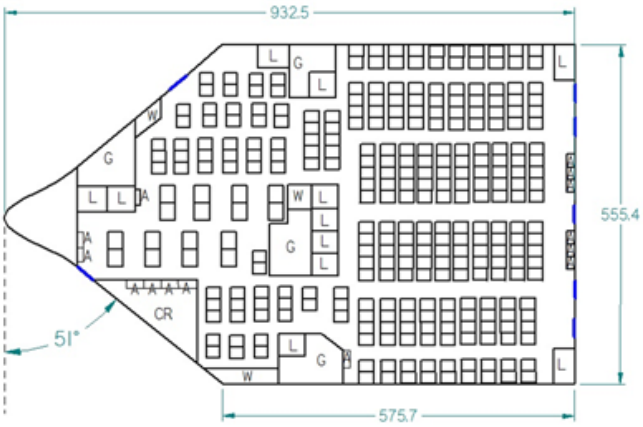

(a) Top view of cabin layout

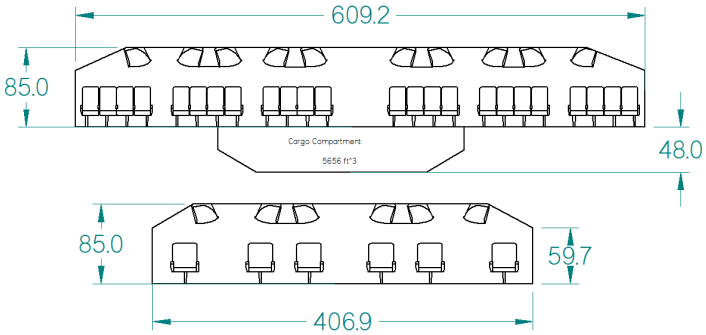

(b) Front view of internal layout of cabin and cargo hold

Figure 7: HWB Cabin layout design for 301 passengers [12]

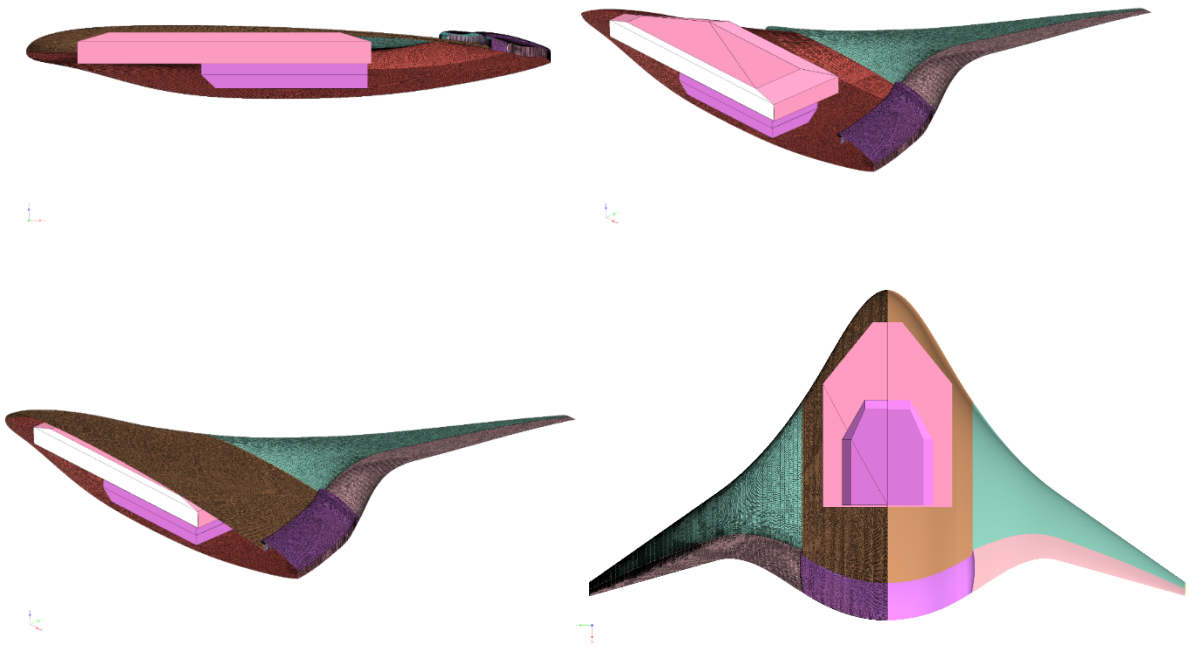

Figure 8: HWB configuration and cabin/cargo hold positioned in the airframe

V. Demonstration of CFD Analysis

The geometry model generated by the present HWB parameterization method can be used as a baseline geometry for unstructured surface and volume meshing for CFD simulations. Computational surface meshes with and without a nacelle is shown Figure 9. Once a computational mesh is generated, it can be deformed for another set of geometric parameters for a fast turnaround time of flow simulation during design optimization process of the HWB airplane.

Go-flow, an inviscid/viscous three dimensional unstructured mesh flow solver, was adopted for flow simulations. In this study, inviscid simulations for Mach 0.84 and angle-of-attack of 3 degrees were conducted for a HWB configuration with and without nacelle on it.

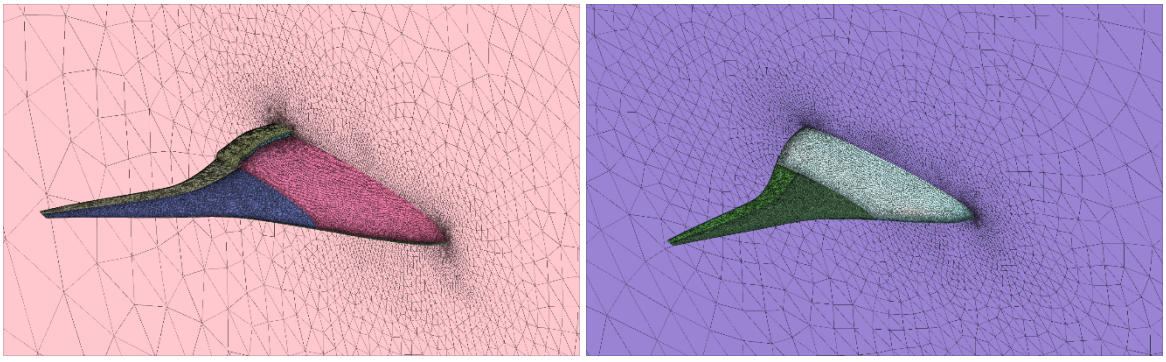

Figure 9: Computational meshes for HWB with and without nacelle

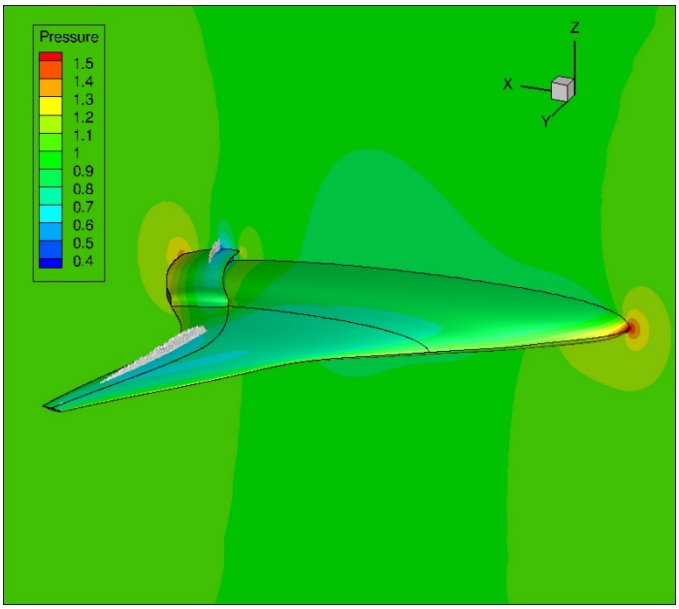

(a) HWB configuration with nacelle

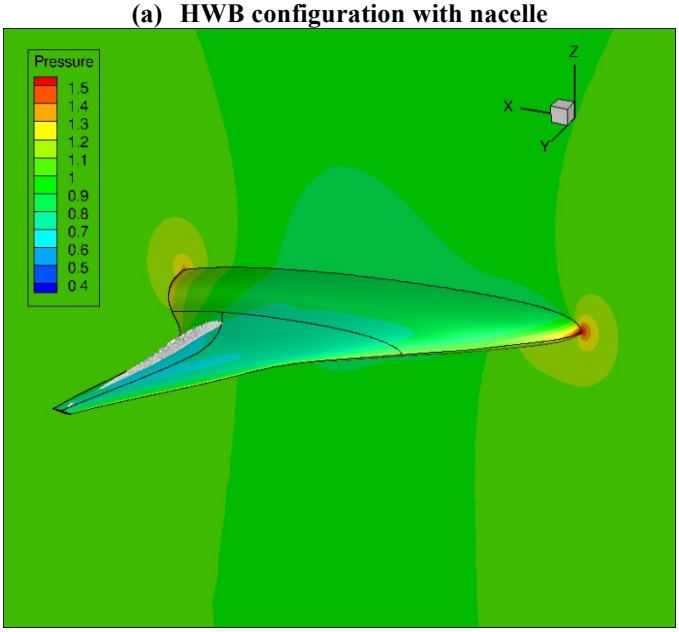

(b) HWB configuration without nacelle

Figure 10: Computed pressure contours for HWB with and without nacelle

Figure 10 shows surface pressure contours and shock wave visualizations for the two configurations. There are shock waves on the outboard upper surface of the airframes. The outboard shock wave extends further inboard for the HWB without nacelle. The HWB with the nacelle has shock wave on the outer cowl surface which was also seen in our previous studies for the N3-X configuration. [9,13]

VI. Conclusions

A design parameterization method for HWB configurations with mail slot nacelle has been developed for a fast exploration of design space in conceptual and preliminary design phases of a HWB configuration. Geometric

constraints for the parameterization such as internal cabin and cargo hold layouts are imposed on the geometry generation. A CFD simulation was performed to demonstrate the analysis for a HWB configuration generated by the current geometric modeler. The results clearly show the significant effect of the nacelle on the flowfield. For future work, the geometric modeling method will be applied to the conceptual design of a HWB configuration with turboelectric distributed propulsion system.

References

[1] Liebeck, R. H., " Design of the Blended Wing Body Subsonic Transport," AIAA J. of Aircraft, Vol. 41, No. 1, 2004.

[2] Dowling, A. and Greitzer, E., "The Silent Aircraft Initiative- Overview," AIAA-2007-0452, Jan. 2007.

[3] Thomas, R. H., Burley, C. L., and Olson, E. D., "Hybrid Wing Body Aircraft System Noise Assessment with Propulsion Airframe Aeroacoustic Experiments," AIAA 2010-3913.

[4] Lyu, Z. and Martins, J., "Aerodynamic Design Optimization Studies of a Blended-Wing-Body aircraft, " J. of Aircraft, Vol. 51, No. 5, 2014.

[5] Liou, M.-S. And Lee, B. J., "Minimizing Inlet Distortion for Hybrid Wing Body Aircraft," J. Turbomachinery, 134, May 2012.

[6] Chima, R. V., "Rapid Calculations of Three-Dimensional Inlet/Fan Interaction," NASA Fundamental Aeronautics 2007 Annual Meeting, New Orleans, LA, Oct. 30–Nov. 1, 2007.

[7] Liou, M.-S., Kim, H. and Liou, M.-F., "Challenges and Progress in Aerodynamic Design of Hybrid Wingbody Aircraft with Embedded Engines," NASA/TM-2014-218309.

[8] Felder, J., Kim, H. D., and Brown, G. V., "An Examination of the Effects of Boundary Layer Ingestion on Turboelectric Distributed Propulsion Systems," AIAA–2011–300, AIAA, 2011.

[9] Kim, H. and Liou, M.-S., "Flow Simulation of N3-X Hybrid Wing-Body Configuration," AIAA 2013-0221.

[10] Kulfan, B., "Universal Parametric Geometry Representation Method," Journal of Aircraft, Vol. 45, No. 1, 2008.

[11] Laughlin, T. W., Corman, J. A., and Mavris, D. N., "A Parametric and Physics-Based Approach to Structural Weight Estimation of the Hybrid Wing Body Aircraft," AIAA 2013-1082, 51st AIAA Aerospace Sciences Meeting, Grapevine, TX, Jan. 2013.

[12] Nickol, C. L., "Hybrid Wing Body Configuration Scaling Study," AIAA 2012-0337, 50th AIAA Aerospace Sciences Meeting, Nashville, TN, Jan. 2012.

[13] Kim, H., Liou, M.-F. and Liou, M.-S. "Mail-Slot Nacelle Shape Design for N3-X Hybrid Wing Body Configuration," AIAA 2015-3805, AIAA Propulsion & Energy Forum 2015, Orlando, FL, 27-29 July 2015.

Appendix A

We applied a piecewise splining algorithm specifically suited for this aircraft. The algorithm splines through given four control points $T_i(x_i,y_i)$, i = 1, 2, 3, 4 in the x-y plane.

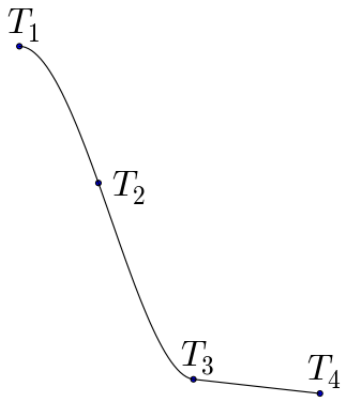

Figure A1: A piecewise splining algorithm through four points

In the derivation, y will be presented as a function of x. In the planform and airfoil loft of the above, x was a function of y. Simply input x from the aircraft into y for the algorithm, and vice versa, to solve for the splines.

The function $f(x)$ is composed of three polynomials, of the format described below.

$$S_1(x) = a_1 + b_1(x - x_1) + c_1(x - x_1)^2 + d_1(x - x_1)^3 \quad \text{(A1)}$$
$$S_2(x) = a_2 + b_2(x - x_2) + c_2(x - x_2)^2 + d_2(x - x_2)^3 \quad \text{(A2)}$$
$$S_3(x) = mx + k \quad \text{(A3)}$$

Spline S_i connects points T_i and T_{i+1}.

The third spline can be readily solved from T_3 and T_4.

$$m = \frac{y_4 - y_3}{x_4 - x_3} \quad \text{(A4)}$$
$$k = y_4 - mx_4 \quad \text{(A5)}$$

The first two splines are cubic piecewise interpolating splines with clamped end conditions. There are eight unknowns in Eqs. (A1) and (A2), so eight rules will be used to define them. It is convenient to use $h_i = x_{i+1} - x_i$.

1. The slope of spline one must be zero at x_1

$$S_1'(x_1) = b_1 = 0 \quad \text{(A6)}$$

2. The slope of spline two at x_3 must equal the slope of spline three.

$$S_2'(x_3) = b_2 + 2c_2h_2 + 3d_2h_2^2 = m = S_3'(x_3) \quad \text{(A7)}$$

3. The slope of spline two must equal the slope of spline one at x_2

$$S_2'(x_2) = S_1'(x_2) \quad \text{(A8)}$$
$$b_2 = b_1 + 2c_1h_1 + 3d_1h_1^2 \quad \text{(A9)}$$
$$b_1 + 2c_1h_1 + 3d_1h_1^2 - b_2 = 0 \quad \text{(A10)}$$

4. The second derivate of spline two must equal the second derivative of spline one at x_2

$$S_2''(x_2) = S_1''(x_2) \quad \text{(A11)}$$
$$2c_2 = 2c_1 + 6d_1h_1 \quad \text{(A12)}$$
$$2c_1 + 6d_1h_1 - 2c_2 = 0 \quad \text{(A13)}$$

5. The value of spline one at x_1 must equal y_1

$$S_1(x_1) = a_1 = y_1 \quad \text{(A14)}$$

6. The value of spline one at x_2 must equal y_2

$$S_1(x_2) = a_1 + b_1h_1 + c_1h_1^2 + d_1h_1^3 = y_2 \quad \text{(A15)}$$

7. The value of spline two at x_2 must equal y_2

$$S_2(x_2) = a_2 = y_2 \quad \text{(A16)}$$

8. The value of spline two at x_3 must equal y_3

$$S_2(x_3) = a_2 + b_2h_2 + c_2h_2^2 + d_2h_2^3 = y_3 \quad \text{(A17)}$$

These equations are all correctly formatted to create a linear system of equations.

$$\begin{bmatrix} 0 & 1 & 0 & 0 & 0 & 0 & 0 & 0 \\ 0 & 0 & 0 & 0 & 0 & 1 & 2h_2 & 3h_2^2 \\ 0 & 1 & 2h_1 & 3h_1^2 & 0 & -1 & 0 & 0 \\ 0 & 0 & 2 & 6h_1 & 0 & 0 & -2 & 0 \\ 1 & 0 & 0 & 0 & 0 & 0 & 0 & 0 \\ 1 & h_1 & h_1^2 & h_1^3 & 0 & 0 & 0 & 0 \\ 0 & 0 & 0 & 0 & 1 & 0 & 0 & 0 \\ 0 & 0 & 0 & 0 & 1 & h_2 & h_2^2 & h_2^3 \end{bmatrix} \begin{bmatrix} a_1 \\ b_1 \\ c_1 \\ d_1 \\ a_2 \\ b_2 \\ c_2 \\ d_2 \end{bmatrix} = \begin{bmatrix} 0 \\ m \\ 0 \\ 0 \\ y_1 \\ y_2 \\ y_2 \\ y_3 \end{bmatrix} \tag{A18}$$

Solving this system of equations will yield the correct coefficients for the cubic piecewise interpolating splines. The complete spline function follows rules that conform well to the outer curvature of the aircraft.

It was found that the above algorithm results in non-realistic curves for trailing edges when the spanwise coordinates of control points T2 and T3 are close each other. For a more robust shape design, the order of the first polynomial S1 for the trailing edge spline curve was reduced from cubic to quadratic by setting the condition 4 as

$$d_1 = 0, \tag{A19}$$

and modifying the matrix equation (A18) accordingly. Figure A2 compares the effect of modified spline method on the resulting trailing edge curve.

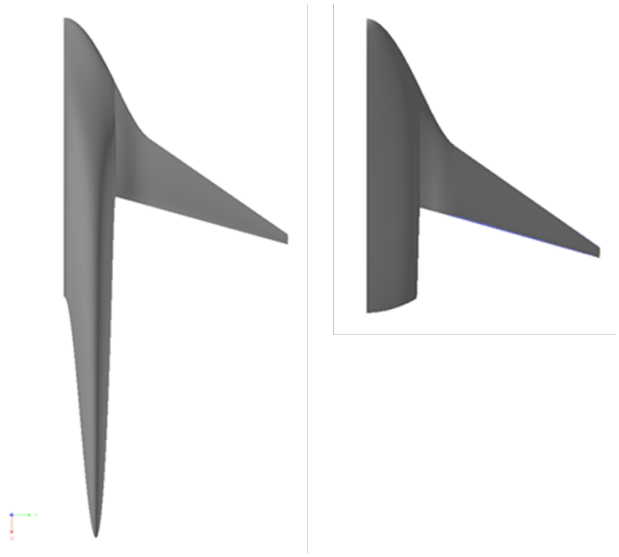

Figure A2: Unrealistic trailing edge curve (left) obtained when control point P3 is located too close to P2 in the spanwise coordinate (left figure: cubic function for S_1, right figure: quadratic function for S_1)